Nano Research

Open Access

Research Article

Anti-thermal quenching upconversion luminescence of Cr^{3+} in $Sc_2(WO_4)_3$:Yb/Cr

Yang Wei[1,3,§], Shuaihao Wu[1,§], Ran Chen[1], Chao Sun[1], Feng Wang[1], Xinru Ding[1], Hui Wang[1], Yanqing Lu[3] ✉, and Ling Huang[1,2] ✉

[1] *School of Chemistry and Molecular Engineering, Nanjing Tech University, Nanjing 211816, China*
[2] *State Key Laboratory of Chemistry and Utilization of Carbon Based Energy Resources, College of Chemistry, Xinjiang University, Urumqi 830017, China*
[3] *College of Engineering and Applied Sciences, Nanjing University, Nanjing 210023, China*
§ *Yang Wei and Shuaihao Wu contributed equally to this work.*

Cite this article: *Nano Research*, **2025**, *18*, 94907097. https://doi.org/10.26599/NR.2025.94907097

ABSTRACT: Although widely need from various applications, the luminescence of Cr^{3+} is easily prone to thermal quenching (TQ), causing remarkable intensity reduction as temperature rises, and posing a significant constraint in applications such as high-power lighting, solid-state lasers, and high-temperature optical sensing. Numerous strategies have been reported to realize anti-thermal quenching luminescence (ATQL) of Cr^{3+}. However, researches into anti-thermal quenching upconversion luminescence (ATQUL) of Cr^{3+} are barely seen. Herein, taking advantage of the enhanced luminescence of Yb^{3+} facilitated by the Frenkel defects formed within $Sc_2(WO_4)_3$ (SWO) matrix upon heating, we have established $Yb^{3+} \rightarrow Cr^{3+}$ cooperative sensitization pathway for upconversion luminescence of Cr^{3+}, and achieved ATQUL of Cr^{3+} in SWO:Yb/Cr. Our findings have not only offered novel perspectives for medium to high-temperature applications of Cr^{3+}-based phosphors, the design principles are also extendable to other transition metal ions.

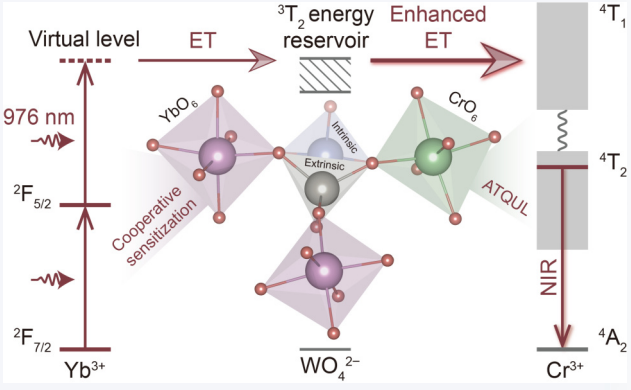

KEYWORDS: Cr^{3+}, $Sc_2(WO_4)_3$, anti-thermal quenching, upconversion luminescence, luminescence thermometry

1 Introduction

The luminescence of Cr^{3+} has drawn widespread attention due to its characteristic broad-band emission, long lifetime, as well as high quantum yield [1–4]. Moreover, Cr^{3+} luminescence is sensitive to its local chemical environment such as temperature, pressure, and external stress [5–10]. Therefore, by manipulating parameters such as host materials, doping behavior (site occupation, co-doped ions, concentration), and synthetic processes (sintering temperature and time), the luminescence of Cr^{3+} can be tuned on demand [11–13]. Unfortunately, like other analogous, the luminescence of Cr^{3+} also suffers from severe thermal quenching (TQ), i.e., the intensity decreases at increased temperatures [14–17]. Although strategies to anti-thermal quenching luminescence (ATQL) have been successively reported, such as enhanced matrix structural rigidity [18–20], trap-assisted mechanisms [21, 22], ion co-doping [23–25], and multi-site occupation [26, 27], studies on anti-thermal quenching upconversion luminescence (ATQUL) of Cr^{3+} are still lacking.

Different from lanthanide ions (Ln^{3+}), transition metal ions like Cr^{3+} has a $3d^n$ electron configuration with three-dimensional orbitals directly exposed to ligands, rendering responsive luminescence to the local coordination environment. Considering the merits of Cr^{3+} that is easily tunable and broad near-infrared (NIR) emission when located at the center of a weak octahedral crystal field [28–30], realization of ATQUL of Cr^{3+} possesses great potential in areas such as photothermal therapy, lasing, and optical sensing. However, current research on ATQUL is limited to Ln^{3+}, and it is important to search for new principles that enable Cr^{3+}-based ATQUL.

Herein, by combining the (i) Frenkel defect (FD) formed in

Received: August 23, 2024; **Revised:** October 17, 2024
Accepted: October 28, 2024

✉Address correspondence to Yanqing Lu, yqlu@nju.edu.cn; Ling Huang, iamlhuang@njtech.edu.cn

$Sc_2(WO_4)_3$ (SWO) crystal lattice, which first absorbs and stores the excitation energy and then releases to doped Yb^{3+} at elevated temperatures [15], and (ii) the perfectly matched energy levels between the virtual energy level formed by Yb^{3+} ion pair and $^4T_1$ of Cr^{3+}, we have realized for the first time, very good ATQUL of Cr^{3+} in SWO:Yb/Cr from 300 to 460 K, with a 16-fold enhancement. As a proof-of-concept of this specially designed material, a high-performance ratiometric luminescence thermometer is fabricated, which shows outstanding absolute (S_a) and relative sensitivity (S_r) of 7.4% K^{-1} and 4% K^{-1}, respectively. This work has greatly pushed forward studies on ATQUL from both fundament and applications of Cr^{3+}-based phosphors, the embedded design principle shall also be extended to other transition metal ions.

2 Experimental

2.1 Chemicals

Sc_2O_3 (99.9%), Yb_2O_3 (99.9%), Er_2O_3 (99.9%), $Gd(NO_3)_3$ and $Yb(NO_3)_3$ were purchased from Beijing HWRK Chem. Co. LTD. $Na_2WO_4{\cdot}2H_2O$, Cr_2O_3 (99.9%) and WO_3 (99.9%) were purchased from Anhui Senrise Technologies Co., Ltd. All the chemicals were used as received without further purification.

2.2 Synthesis of SWO:A (A = Yb^{3+}, Er^{3+}, Cr^{3+})

In a typical synthesis of SWO:Yb/Cr (8/0.1 mol%), accurately weigh the following raw materials on an electronic balance based on specific stoichiometric ratios: 0.919 mmol of Sc_2O_3, 0.08 mmol of Yb_2O_3, 0.001 mmol of Cr_2O_3, and 3 mmol of WO_3. Next, transfer these raw materials into an agate mortar and grind them together for 30 min to ensure thorough mixing. Then, transfer the well-mixed powder into a high-temperature resistant alumina crucible. Place the crucible containing the raw materials into a muffle furnace at 1100 °C and maintain at this temperature for 6 h. After the reaction is complete, cool it to room temperature, and grind it again for 30 min to obtain finely homogeneous phosphor. Finally, collect the powder in a 5 mL centrifuge tube for subsequent use. SWO:Yb/Cr (x/0.1 mol%) (x = 2, 4, 6, 8, 10) and SWO:Er (2 mol%) were synthesized by the same methods, where only the addition of raw materials were changed accordingly.

2.3 Synthesis of $Gd_2(WO_4)_3$:Yb

In a typical synthesis of $Gd_2(WO_4)_3$:Yb (8 mol%), 1.84 mmol of $Gd(NO_3)_3$ and 0.16 mmol of $Yb(NO_3)_3$ were added to 40 mL of distilled water under magnetic stirring. After being mixed for 15 min, 3 mmol $Na_2WO_4{\cdot}2H_2O$ was added and then agitated for 30 min. The resulting precipitates were separated by centrifugation at 8000 rpm, washed with deionized water for 10 min, dried at 70 °C in air for 2 h, and finally annealed at 1100 °C for 6 h. After the reaction is complete, cool it to room temperature, and grind it again for 30 min to obtain finely homogeneous phosphor. Finally, collect the powder in a 5 mL centrifuge tube for subsequent use.

2.4 Synthesis of SWO:Er & SWO:Yb/Cr composites

Accurately weigh phosphor samples of SWO:Er (2 mol%) and SWO:Yb/Cr (8 mol%/0.1 mol%) in a 2:1 mass ratio, and place them into a 20 mL beaker. Add 10 mL of ethanol and a magnetic stir bar into the beaker. Stir the mixture at 1500 rpm for 12 h on a magnetic stirrer to ensure complete mixing. Subsequently, position the beaker on a magnetic stirrer equipped with heating functionality, set the temperature to 50 °C, and maintain stirring at 1000 rpm until all the ethanol has fully evaporated. Finally, place the beaker in an oven and dry at 80 °C for 6 h to eliminate any remaining ethanol. After drying, grind the samples uniformly and store them in small centrifuge tubes for further use.

2.5 Characterizations

X-ray diffraction (XRD) was carried out on a Rigaku D/max 2550 diffractometer using monochromatized Cu Kα radiation (λ = 0.15418 nm) and the measurement were performed in the range of 2θ = 10°–80° with 0.02 °/step. Scanning electron microscopy (SEM) images were recorded on a Hitachi SU8220 field emission scanning electron microscope (Hitachi High-Tech Co., Ltd.). Both upconversion and downshifting luminescence spectra were recorded on Edinburgh FLS1000 spectrometer equipped with an external continuous wave diode 488 and 980 nm laser. The sample was heated from 300 to 1100 K on a heating plat (HRTS-1000, Shanghai Hui Tong Optical Instrument Co., Ltd.). The temperature-dependent (300–500 K) luminescence spectra were collected in a cryostat (Optistat DN2, Oxford Instruments). The decay curves were measured on an Edinburgh FLS1000 fluorescence spectrometer equipped with a pulse modulator controlled 980 nm diode laser.

3 Results and discussion

Orthorhombic SWO is composed of corner-sharing ScO_6 octahedra and WO_4 tetrahedra, at the center of which, Sc and W locate, respectively (Fig. 1(a), and Figs. S1 and S2 in the Electronic Supplementary Material (ESM)). Sc^{3+} sites will be replaced when the activator Cr^{3+} and sensitizer Yb^{3+} ions are doped in SWO, which is vital for realizing Yb^{3+} sensitized UCL of Cr^{3+}.

When heated, partial intrinsic WO_4 tetrahedra become distorted and form extrinsic WO_4 (Fig. 1(b) and Fig. S3 in the ESM), which well agrees with the two emission centers in Fig. 1(c). Overlap of both molecular orbitals forms the FD, which functions as energy reservoir by absorbing and storing the excitation energy at 976 nm through the Yb^{3+} → FD energy transfer (ET), as depicted in Fig. 1(d) [15]. Subsequently, the stored energy will be released upon heating and then back-transferred to Yb^{3+}, the amount of which well surpasses that depleted by TQ so that ATQL of Yb^{3+} can be easily obtained (Fig. 1(e)). As a stark contrast, only one emission peak is detected in the emission spectra (Fig. 1(f)) of monoclinic $Gd_2(WO_4)_3$ (GWO), which suggests only one type of WO_4 tetrahedron, and thus no FD can be formed in GWO:Yb (Fig. 1(g)). So, there is no energy reservoir functionality in GWO, and only monotonous TQ of Yb^{3+} is obtained (Fig. 1(h)). The mechanisms corresponding to ATQL and TQ of Yb^{3+} in SWO and GWO are illustrated in Figs. 1(d) and 1(g), respectively.

It is well known that luminescence of Cr^{3+} is closely related to the local crystal field environment [28]. When doped into Sc^{3+} site that located at the center of the octahedron, the excitation spectrum of Cr^{3+} in SWO:Cr (0.1 mol%) comprises two peaks located at 488 and 700 nm (Fig. 2(a)), corresponding to the $^4A_2$ → $^4T_1$ and $^4A_2$ → $^4T_2$ transitions of Cr^{3+}, respectively.

The Dq/B value calculated from excitation spectrum of SWO:Cr (0.1 mol%) is less than 2.3, indicating that Cr^{3+} sits in a weak crystal field (Fig. 2(b) and Eq. S1 in the ESM). Under this circumstance, the lowest excitation energy level is $^4T_2$ and the spin-allowed $^4T_2$ → $^4A_2$ transition occurs. Therefore, under 488 nm excitation, electrons in the $^4A_2$ ground level will be excited to the $^4T_1$ level and then

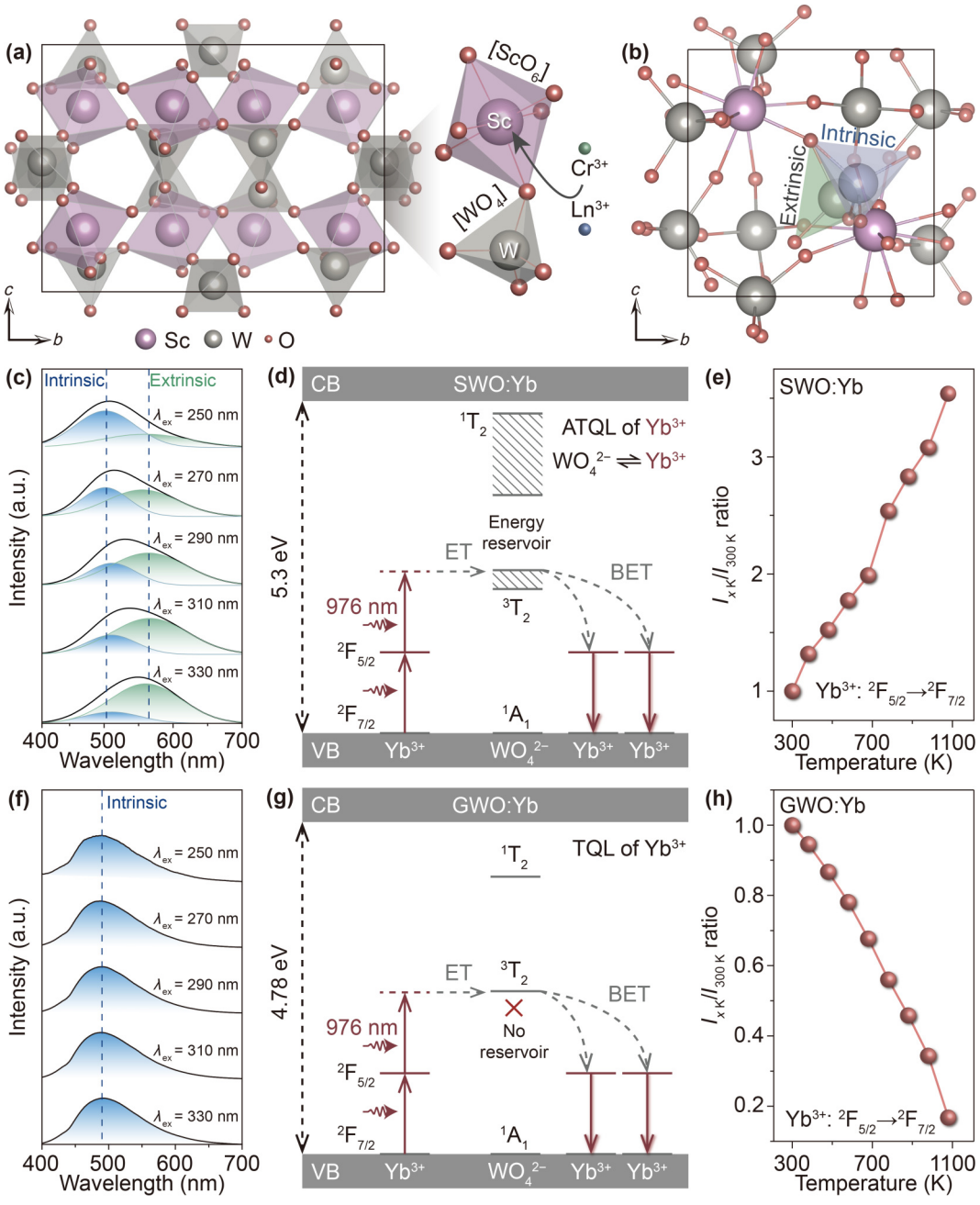

Figure 1 Frenkel defect-modulated ATQL of Yb^{3+} in SWO. (a) Crystal structure of SWO. (b) Distortion of intrinsic WO_4^{2-} (blue tetrahedra) to extrinsic WO_4^{2-} (green tetrahedra) forms FD. (c) Wavelength-dependent emission spectra of SWO. (d) ET pathways inside SWO:Yb (8 mol%). (e) Temperature-dependent luminescence intensity ratio $I_{xK}/I_{293\,K}$ of Yb^{3+} in SWO:Yb (8 mol%). (f) Wavelength-dependent emission spectra of GWO. (g) ET pathways inside GWO:Yb (8 mol%). (h) Temperature-dependent luminescence intensity ratio $I_{xK}/I_{293\,K}$ of Yb^{3+} in GWO:Yb (8 mol%).

undergo a non-radiative relaxation to the $^4T_2$ energy level. These electrons subsequently emit downshifting NIR luminescence ranging from 700 to 1200 nm upon returning to the $^4A_2$ level (Fig. S4 in the ESM). More importantly, the 488 nm excitation coincidently matches the virtual energy level formed by the Yb^{3+} ion pair, which then transfers the excitation energy to the $^4T_1$ level of Cr^{3+} through cooperative sensitization [31, 32], generating NIR UCL of Cr^{3+} (Fig. 2(c)), and also forms the basis for realizing ATQUL of Cr^{3+}. To avoid the influence of the 976 nm excitation signal on the NIR UCL of Cr^{3+}, an 800 nm short-pass filter was used at the testing end, thus shifting the NIR emission of Cr^{3+} to 750 nm (Fig. S5 in the ESM).

Control experiment suggests 8 mol% is the optimal doping concentration of Yb^{3+} for realizing UCL of Cr^{3+} in SWO:Yb/Cr (x mol%/0.1 mol%) (x = 2, 4, 6, 8, 10) (Figs. S5–S7 in the ESM). Power-dependent spectra prove a two-photon upconversion mechanism in SWO:Yb/Cr (8 mol%/0.1 mol%) (Fig. 2(d) and Fig. S8 in the ESM). The detected slope of 1.88 is less than the theoretical value for a two-phonon process, which shall be due to the large depopulation rate of intermediate energy level in the upconversion process caused by backward ET from Cr^{3+} to Yb^{3+} [33–35].

Based on the above discussion, it can be predicted that the ATQUL of Cr^{3+} shall originate from the ATQL of Yb^{3+} through the Yb^{3+} → Cr^{3+} cooperative sensitization process. As depicted in Fig.

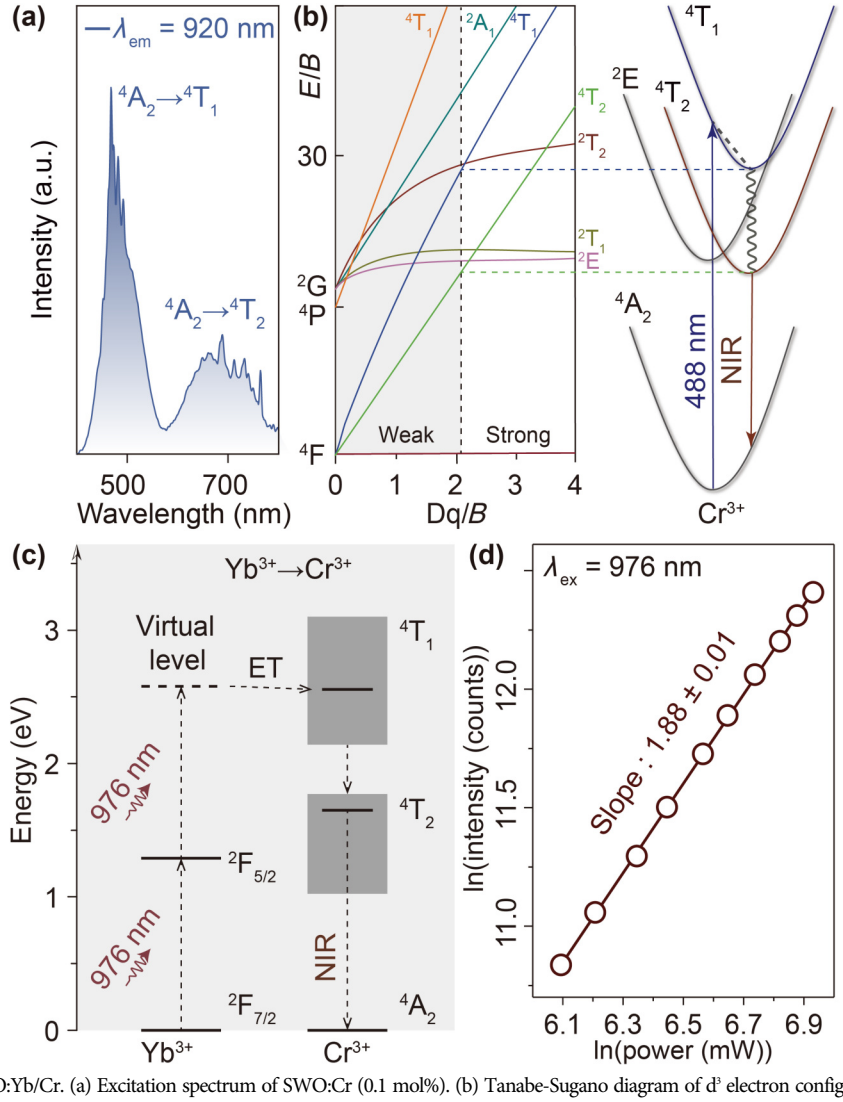

Figure 2 UCL of Cr^{3+} in SWO:Yb/Cr. (a) Excitation spectrum of SWO:Cr (0.1 mol%). (b) Tanabe-Sugano diagram of d^3 electron configuration and ET diagram of Cr^{3+} under 488 nm excitation. (c) Illustration of the cooperative sensitization through $Yb^{3+} \rightarrow Cr^{3+}$ ET in SWO:Yb/Cr (8/0.1 mol%). (d) The log–log plots of UCL intensity of Cr^{3+} vs. excitation power density (λ_{ex} = 976 nm).

3(a), upon 976 nm excitation, the excited electrons at the $^2F_{5/2}$ level can further absorb 976 nm photons and store the excitation energy in the $^3T_2$ energy reservoir in SWO, which will be released upon heating and back-transferred to Yb^{3+}, leading to ATQL of Yb^{3+} (Fig. 1(e) and Fig. S9(a) in the ESM).

Thanks to the perfect energy level match between $^4T_2$ (Cr^{3+}) and $^2F_{5/2}$ (Yb^{3+}), such energy can be further transferred from Yb^{3+} to co-doped Cr^{3+} resulting upconversion emission at 750 nm. Indeed, the apparently dropped luminescence intensity of Yb^{3+} when co-doped with 0.1 mol% Cr^{3+} clearly proves the $Yb^{3+} \rightarrow Cr^{3+}$ ET (Fig. 3(b)), which perfectly consists with the temperature-dependent luminescence intensity shown in Fig. 3(c) and Fig. S9 in the ESM. As shown in Fig. 3(d), the ET efficiency gradually increases from 300 K and reaches a record-high value of 45% at 500 K (Fig. S10 and Table S1 in the ESM), which ensures that the energy transferred to Cr^{3+} well surpasses that depleted by TQ on Cr^{3+}, and forms the origin of ATQUL in SWO:Yb/Cr (8 mol%/0.1 mol%). As expected, unlike the routine TQL of Cr^{3+} under 488 nm excitation without ET from Yb^{3+} (Fig. 3(e) and Fig. S11(a) in the ESM), the UCL intensity of Cr^{3+} in SWO:Yb/Cr (8 mol%/0.1 mol%) continuously increases with temperature, reaching a maximum 16-fold enhancement at 460 K (Fig. 3(e) and Fig. S11(b) in the ESM).

The great ATQUL of SWO:Yb/Cr (8 mol%/0.1 mol%) lays a solid foundation (Table S2 in the ESM) for realizing high-performing optical thermometer working at high-temperature, which can effectively eliminate errors caused by testing environment and instrumentation [36]. Therefore, a composite material system was prepared by mixing SWO:Er (2 mol%) with SWO:Yb/Cr (8 mol%/0.1 mol%). On one hand, the green and NIR emission peaks of Er^{3+} and Cr^{3+} are located between 510–570 and 700–800 nm (Fig. S12 in the ESM), respectively, which effectively avoid temperature sensing errors caused by emission peak overlap. On the other hand, unlike the ATQUL of SWO:Yb/Cr (8 mol%/0.1 mol%), SWO:Er (2 mol%) exhibits normal TQ (Fig. 4(a)). The diametrically opposed thermal-responsive luminescence of Er^{3+} and Cr^{3+} offers a higher response difference than ordinarily used thermally coupled energy levels [37], which renders better thermometric sensitivities.

The thermometric parameter of fluorescence intensity ratio (FIR), which is defined as the intensity ratio of I_1 and I_2, is plotted in Fig. 4(b), exhibits a good exponential relationship at 300–440 K. The calculated maximum S_a and S_r reaches 7.4% K^{-1} (440 K) and

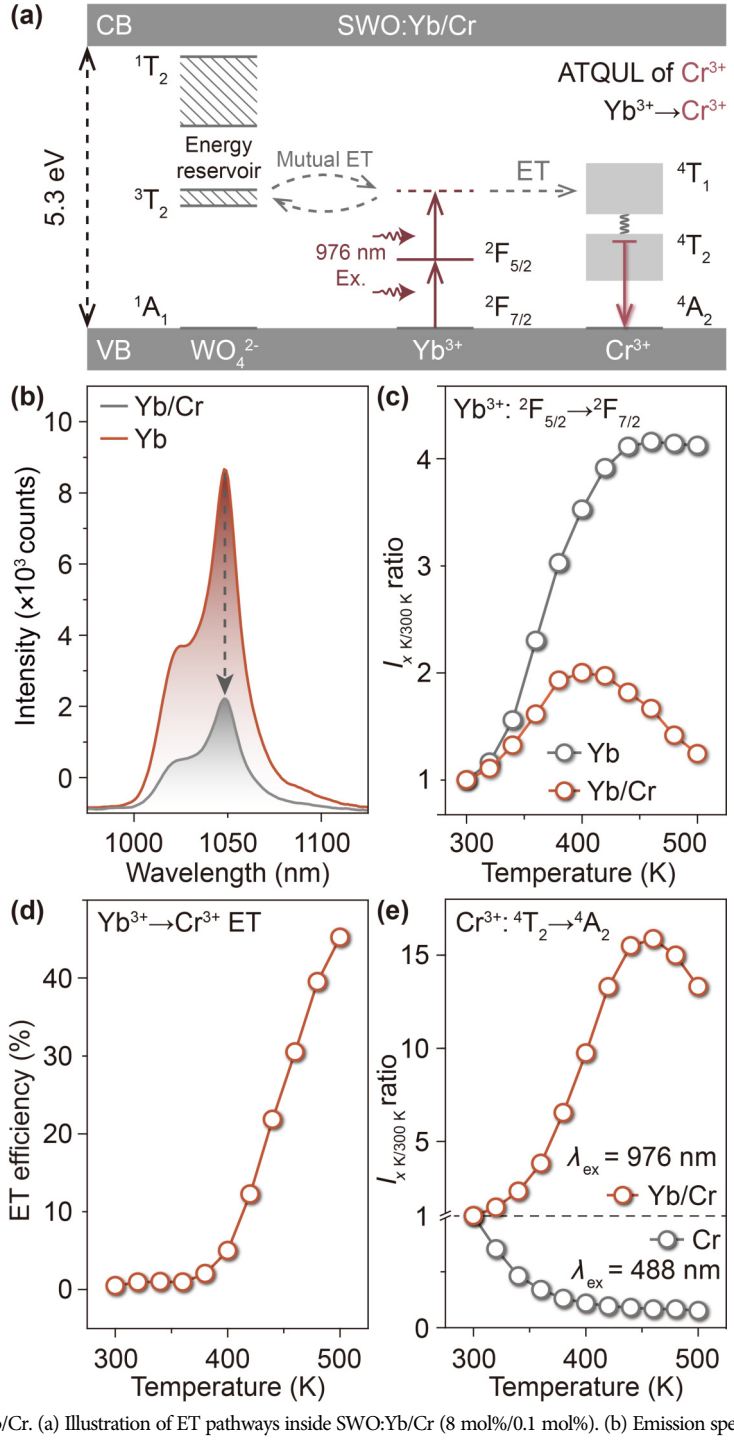

Figure 3 ATQUL of Cr^{3+} in SWO:Yb/Cr. (a) Illustration of ET pathways inside SWO:Yb/Cr (8 mol%/0.1 mol%). (b) Emission spectra of Yb^{3+} in SWO:Yb (8 mol%) and SWO:Yb/Cr (8 mol%/0.1 mol%). (c) Comparison of the temperature-dependent integrated intensity ratio $I_{x\ K/300\ K}$ of Yb^{3+} in SWO:Yb (8 mol%) and SWO:Yb/Cr (8 mol%/0.1 mol%). Temperature-dependent (d) Yb^{3+}-Cr^{3+} ET efficiency in SWO:Yb/Cr (8 mol%/0.1 mol%) and (e) integrated intensity ratio $I_{x\ K/300\ K}$ of Cr^{3+} in SWO:Yb/Cr (8 mol%/0.1 mol%) under 976 nm (red curve) and SWO:Cr (0.1 mol%) under 488 nm (gray curve) excitations.

4% K^{-1} (300 K), respectively (Fig. 4(c) and Eq. S2 in the ESM), exhibiting great performance and the cyclic test further proves decent reliability of constructed luminescence thermometry (Fig. 4(d)).

4 Conclusions

We have realized for the first time, UCL and further ATQUL of Cr^{3+} in SWO:Yb/Cr, i.e., a 16-fold enhancement was obtained at 460 K compared to that at room temperature. Mechanism studies prove that ATQUL originates from the Frenkel defects formed in SWO, which enables the ATQL of Yb^{3+} and finally ATQUL of Cr^{3+} through a record-high efficient Yb^{3+}-Cr^{3+} cooperative sensitization process. The S_a and S_r of 7.4% K^{-1} and 4% K^{-1} in the as fabricated ratiometric luminescence thermometer demonstrating its excellent temperature sensing performance and stability. Using Cr^{3+} as a prototype, this work extends the study of ATQUL to transition metal ions, which provides a new perspective for realizing ATQUL

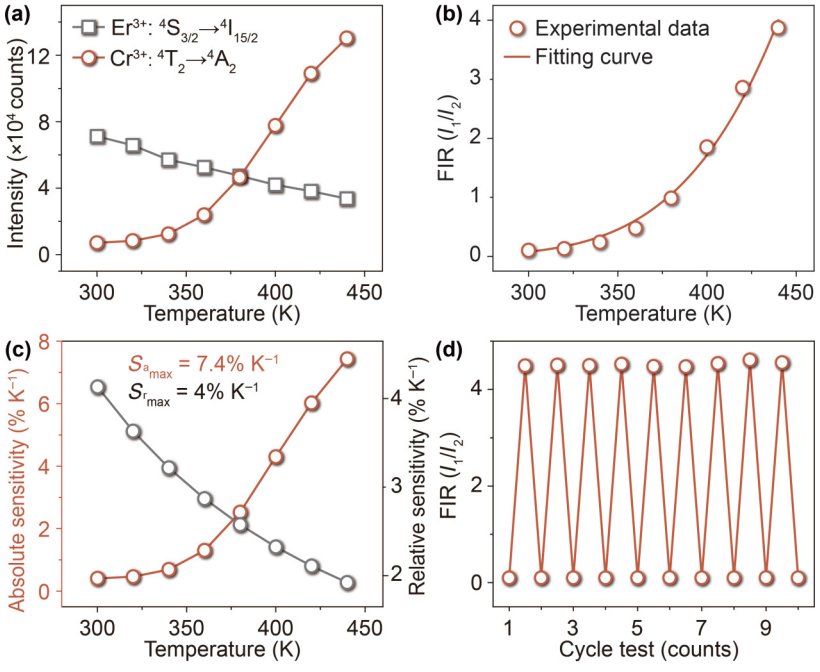

Figure 4 Construction of optical thermometer. (a) Temperature-dependent integrated luminescence intensity corresponding to $^4S_{3/2} \rightarrow {}^4I_{15/2}$ in Er^{3+} (gray curve) and $^4T_2 \rightarrow {}^4A_2$ in Cr^{3+} (red curve) transition, respectively. (b) Calculated temperature-dependent FIR values. (c) Temperature-dependent S_a (red curve) and S_r (gray curve) of constructed luminescence thermometry. (d) Variation of FIR at high and low temperatures over 10 cycles. All the data were measured under 976 nm laser excitation.

at a wider range and will greatly promote derived optical applications.

Electronic Supplementary Material: Supplementary material (further details of structure and composition characterizations, luminescent measurements, and detailed calculations) is available in the online version of this article at https://doi.org/10.26599/NR.2025.94907097.

Data availability

All data needed to support the conclusions in the paper are presented in the manuscript and the Electronic Supplementary Material. Additional data related to this paper may be requested from the corresponding author upon request.

Acknowledgements

This work was supported by the National Key Research and Development Program of China (No. 2022YFA1405000), the National Natural Science Foundation of China (No. 21871137), the Basic Research Program of Jiangsu Province (No. BK20232040), the China Postdoctoral Science Foundation (No. 2024M751381), China National Postdoctoral Program for Innovative Talents (No. BX20240163), Jiangsu Funding Program for Excellent Postdoctoral Talent (No. 2024ZB861), and the Natural Science Foundation of Jiangsu Province (No. BK20243067).

Declaration of competing interest

All the contributing authors report no conflict of interests in this work.

Author contributions

Y. W.: Data curation, experimental design, validation, writing manuscript. S. H. W.: Data curation, validation. R. C.: Data curation, writing manuscript. C. S.: Data curation. F. W.: Data curation. X. R. D.: Validation. H. W.: Validation. Y. Q. L.: Project administration, funding acquisition. L. H.: Conceptualization, project administration, funding acquisition, writing and editing manuscript. All the authors have approved the final manuscript.

Use of AI statement

None.

References

[1] Wang, S. W.; Pang, R.; Tan, T.; Wu, H. Y.; Wang, Q.; Li, C. Y.; Zhang, S.; Tan, T. X.; You, H. P.; Zhang, H. J. Achieving high quantum efficiency broadband NIR $Mg_4Ta_2O_9$: Cr^{3+} phosphor through lithium-ion compensation. *Adv. Mater.* **2023**, *35*, 2300124.

[2] Xiao, W. E.; Basore, E. T.; Zheng, G. J.; Liu, X. F.; Xu, B. B.; Qiu, J. R. Suppressed concentration quenching brightens short-wave infrared emitters. *Adv. Mater.* **2023**, *35*, 2306517.

[3] Zhong, C. S.; Xu, Y. H.; Wu, X. D.; Yin, S. W.; Zhang, X. B.; Zhou, L.; You, H. P. High output power and high quantum efficiency in novel NIR phosphor $MgAlGa_{0.7}B_{0.3}O_4$:Cr^{3+} with profound FWHM variation. *Adv. Mater.* **2024**, *36*, 2309500.

[4] Liu, G. C.; Chen, W. B.; Xiong, Z.; Wang, Y. Z.; Zhang, S.; Xia, Z. G. Laser-driven broadband near-infrared light source with watt-level output. *Nat. Photonics* **2024**, *18*, 562–568.

[5] Healy, S. M.; Donnelly, C. J.; Glynn, T. J.; Imbusch, G. F.; Morgan, G. P. Temperature dependence of the luminescence of GSGG:Cr^{3+}. *J. Lumin.* **1990**, *46*, 1–7.

[6] Ristić, Z.; Đorđević, V.; Medić, M.; Kuzman, S.; Brik, M. G.; Antić, Ž.; Dramićanin, M. D. Temperature dependence of the Cr^{3+}-DOPED Mg_2TiO_4 near-infrared emission. *Opt. Mater.* **2021**, *120*, 111468.

[7] Back, M.; Ueda, J.; Hua, H. S.; Tanabe, S. Predicting the optical pressure sensitivity of $^2E \rightarrow {}^4A_2$ spin-flip transition in Cr^{3+}-doped crystals. *Chem. Mater.* **2021**, *33*, 3379–3385.

[8] Szymczak, M.; Runowski, M.; Brik, M. G.; Marciniak, L. Multimodal, super-sensitive luminescent manometer based on giant pressure-induced spectral shift of Cr^{3+} in the NIR range. *Chem. Eng. J.* **2023**, *466*, 143130.

[9] Liu, S. Q.; Zheng, Y. T.; Peng, D. F.; Zhao, J.; Song, Z.; Liu, Q. L. Near-infrared mechanoluminescence of Cr^{3+} doped gallate spinel and magnetoplumbite smart materials. *Adv. Funct. Mater.* **2022**, *33*, 2209275.

[10] Liu, Z. C.; Yu, X.; Peng, Q. P.; Zhu, X. D.; Xiao, J. Q.; Xu, J. T.; Jiang, S. X.; Qiu, J. B.; Xu, X. H. NIR mechanoluminescence from Cr^{3+} activated $Y_3Al_5O_{12}$ with intense zero phonon line. *Adv. Funct. Mater.* **2023**, *33*, 2214497.

[11] Jia, Z. W.; Yuan, C. X.; Liu, Y. F.; Wang, X. J.; Sun, P.; Wang, L.; Jiang, H. C.; Jiang, J. Strategies to approach high performance in Cr^{3+}-doped phosphors for high-power NIR-LED light sources. *Light Sci. Appl.* **2020**, *9*, 86.

[12] Dang, P. P.; Wei, Y.; Liu, D. J.; Li, G. G.; Lin, J. Recent advances in chromium-doped near-infrared luminescent materials: Fundamentals, optimization strategies, and applications. *Adv. Opt. Mater.* **2023**, *11*, 2201739.

[13] Zhao, F. Y.; Song, Z.; Liu, Q. L. Advances in chromium-activated phosphors for near-infrared light sources. *Laser Photonics Rev.* **2022**, *16*, 2200380.

[14] Wei, Y.; Liu, Z. N.; Sun, C.; Ding, X. R.; Wu, S. H.; Chen, R.; Wang, F.; Wang, H.; Xing, X. R.; Huang, L. Tunable anti-thermal quenching luminescence of Eu^{3+}-doped metal-organic framework and temperature-dependent photonic coding. *Adv. Funct. Mater.* **2024**, *34*, 2401664.

[15] Wei, Y.; Pan, Y.; Zhou, E. L.; Yuan, Z.; Song, H.; Wang, Y. L.; Zhou, J.; Rui, J. H.; Xu, M. J.; Ning, L. X. et al. Frenkel defect-modulated anti-thermal quenching luminescence in lanthanide-doped $Sc_2(WO_4)_3$. *Angew. Chem., Int. Ed.* **2023**, *62*, e202303482.

[16] Wang, Y. L.; Rui, J. H.; Song, H.; Yuan, Z.; Huang, X. Q.; Liu, J. Y.; Zhou, J.; Li, C.; Wang, H.; Wu, S. H. et al. Antithermal quenching upconversion luminescence via suppressed multiphonon relaxation in positive/negative thermal expansion core/shell $NaYF_4$:Yb/Ho@ScF_3 nanoparticles. *J. Am. Chem. Soc.* **2024**, *146*, 6530–6535.

[17] Zheng, R.; Wei, Y.; Zhang, Z. C.; Wang, Z. Y.; Ma, L. L.; Wang, Y.; Huang, L.; Lu, Y. Q. Stimuli-responsive active materials for dynamic control of light field. *Responsive Mater.* **2023**, *1*, e20230017.

[18] Xu, X. X.; Shao, Q. Y.; Yao, L. Q.; Dong, Y.; Jiang, J. Q. Highly efficient and thermally stable Cr^{3+}-activated silicate phosphors for broadband near-infrared LED applications. *Chem. Eng. J.* **2020**, *383*, 123108.

[19] Wen, D. W.; Liu, H. M.; Guo, Y.; Zeng, Q. G.; Wu, M. M.; Liu, R. S. Disorder-order conversion-induced enhancement of thermal stability of pyroxene near-infrared phosphors for light-emitting diodes. *Angew. Chem., Int. Ed.* **2022**, *61*, e202204411.

[20] Xie, J. H.; Tian, J. H.; Jiang, L. P.; Cao, M.; Zhuang, W. D. An efficient and thermally stable Cr^{3+}-activated $Y_2GdSc_2Al_2GaO_{12}$ garnet phosphor for NIR spectroscopy applications. *Dalton Trans.* **2023**, *52*, 15950–15957.

[21] Lin, H. H.; Bai, G. X.; Yu, T.; Tsang, M. K.; Zhang, Q. Y.; Hao, J. H. Site occupancy and near-infrared luminescence in $Ca_3Ga_2Ge_3O_{12}$: Cr^{3+} persistent phosphor. *Adv. Opt. Mater.* **2017**, *5*, 1700227.

[22] Zhang, H. X.; Wei, J. L.; Chen, W.; Mao, Y. B. Near-infrared-emitting $K_2CaP_2O_7$:Cr^{3+} with outstanding thermal stability. *ACS Appl. Opt. Mater.* **2023**, *1*, 1595–1604.

[23] Wu, X. D.; Zhao, S.; Zhang, L.; Dong, L. P.; Xu, Y. H.; Yin, S. W.; You, H. P. Highly thermally stable Cr^{3+} and Yb^{3+} codoped Gd_2GaSbO_7 phosphors for broadband near-infrared applications. *Dalton Trans.* **2021**, *50*, 13459–13467.

[24] Lang, T. C.; Zhao, Q. Y.; Jing, X. L.; Guan, G. X. Y.; Fang, S. Q.; Qiang, Q. P.; Peng, L. L.; Han, T.; Yakovlev, A. N.; Liu, B. T. Highly efficient near-infrared solid solution phosphors with excellent thermal stability and tunable spectra for pc-LED light sources toward NIR spectroscopy applications. *Phys. Chem. Chem. Phys.* **2023**, *25*, 25985–25992.

[25] Ouyang, S.; Yin, J. M.; Su, L. J.; Yao, M. H.; Wang, G. C.; Yang, J. Y.; Molokeev, M. S.; Zhou, Z.; Zhang, S. J.; Xia, M. Highly efficient and thermostable far-red phosphor for promoting root growth in plants. *J. Mater. Chem. C* **2024**, *12*, 3272–3279.

[26] Rajendran, V.; Fang, M. H.; Huang, W. T.; Majewska, N.; Lesniewski, T.; Mahlik, S.; Leniec, G.; Kaczmarek, S. M.; Pang, W. K.; Peterson, V. K. et al. Chromium ion pair luminescence: A strategy in broadband near-infrared light-emitting diode design. *J. Am. Chem. Soc.* **2021**, *143*, 19058–19066.

[27] Yao, L. Q.; Shao, Q. Y.; Shi, M. L.; Shang, T. Q.; Dong, Y.; Liang, C.; He, J. H.; Jiang, J. Q. Efficient ultra-broadband Ga_4GeO_8:Cr^{3+} phosphors with tunable peak wavelengths from 835 to 980 nm for NIR pc-LED Application. *Adv. Opt. Mater.* **2022**, *10*, 2102229.

[28] De Guzman, G. N. A.; Fang, M. H.; Liang, C. H.; Bao, Z.; Hu, S. F.; Liu, R. S. [INVITED] Near-infrared phosphors and their full potential: A review on practical applications and future perspectives. *J. Lumin.* **2020**, *219*, 116944.

[29] Fang, M. H.; Huang, P. Y.; Bao, Z.; Majewska, N.; Leśniewski, T.; Mahlik, S.; Grinberg, M.; Leniec, G.; Kaczmarek, S. M.; Yang, C. W. et al. Penetrating biological tissue using light-emitting diodes with a highly efficient near-infrared $ScBO_3$: Cr^{3+} phosphor. *Chem. Mater.* **2020**, *32*, 2166–2171.

[30] Zhou, Y. P.; Li, X. J.; Seto, T.; Wang, Y. H. A high efficiency trivalent chromium-doped near-infrared-emitting phosphor and its NIR spectroscopy application. *ACS Sustain. Chem. Eng.* **2021**, *9*, 3145–3156.

[31] Cheng, X. W.; Zhou, J.; Yue, J. Y.; Wei, Y.; Gao, C.; Xie, X. J.; Huang, L. Recent development in sensitizers for lanthanide-doped upconversion luminescence. *Chem. Rev.* **2022**, *122*, 15998–16050.

[32] Heer, S.; Wermuth, M.; Krämer, K.; Ehrentraut, D.; Güdel, H. U. Up-conversion excitation of sharp Cr^{3+} ^2E emission in YGG and YAG codoped with Cr^{3+} and Yb^{3+}. *J. Lumin.* **2001**, *94–95*, 337–341.

[33] Pollnau, M.; Gamelin, D. R.; Lüthi, S. R.; Güdel, H. U.; Hehlen, M. P. Power dependence of upconversion luminescence in lanthanide and transition-metal-ion systems. *Phys. Rev. B* **2000**, *61*, 3337–3346.

[34] Ye, S.; Li, Y. J.; Yu, D. C.; Dong, G. P.; Zhang, Q. Y. Room-temperature upconverted white light from $GdMgB_5O_{10}$:Yb^{3+}, Mn^{2+}. *J. Mater. Chem.* **2011**, *21*, 3735–3739.

[35] Ye, S.; Song, E. H.; Ma, E.; Zhang, S. J.; Wang, J.; Chen, X. Y.; Zhang, Q. Y.; Qiu, J. R. Broadband Cr^{3+}-sensitized upconversion luminescence in $La_3Ga_5GeO_{14}$:Cr^{3+}, Yb^{3+}, Er^{3+}. *Opt. Mater. Express,* **2014**, *4*, 638–648.

[36] Brites, C. D. S.; Marin, R.; Suta, M.; Carneiro Neto, A. N.; Ximendes, E.; Jaque, D.; Carlos, L. D. Spotlight on luminescence thermometry: Basics, challenges, and cutting-edge applications. *Adv. Mater.* **2023**, *35*, 2302749.

[37] Brites, C. D. S.; Balabhadra, S.; Carlos, L. D. Lanthanide-based thermometers: At the cutting-edge of luminescence thermometry. *Adv. Opt. Mater.* **2019**, *7*, 1801239.